

RHEINISCHE FRIEDRICH-WILHELMS-UNIVERSITÄT BONN

ADVANCED LABORATORY COURSE

PERFORMED ON: APRIL 22, 2022

SUBMITTED ON: MAY 13, 2022

K221: Mößbauer Effect

Authors

Paarth Thakkar
Keito Watanabe

Tutor(s)

Dr. Jens Barth

Abstract

Contents

1	Introduction	2
2	Theoretical Background	3
2.1	Principles	3
2.1.1	Natural Linewidth	3
2.1.2	Recoil and Doppler Shift	4
2.1.3	Debye-Waller Factor	4
2.2	Mößbauer Source	6
2.3	Mößbauer Apparatus and Setup	6
2.4	Isomer Shift	8
2.5	Electric Quadrupole Interaction	9
2.6	Magnetic Dipole Interaction	10
3	Experimental Set-Up	11
4	Calibration	13
5	Moessbauer Spectrum	14
5.1	Spectrum	14
5.2	Natural Linewidth	15
6	Conclusion and Outlook	17
7	Acknowledgements	18
8	Appendix	20

Chapter 1

Introduction

In this experiment, the phenomenon known as Mößbauer effect. is studied by means of transition spectroscopy. Using a ^{57}Co source, this effect is observed and the hyperfine structure of 14.4 keV transition in ^{57}Fe is measured.

From the Mößbauer spectrum of measured, we can see the isomeric shift and quadrupole and magnetic splitting of energy levels. Using this, one can determine the *g*-factor of the ground state and the first excited state can be determined.

Chapter 2

Theoretical Background

In the following section, we shall study the theoretical background of the Mößbauer effect in brief. A much more detailed discussion can be found in [1], mostly on which the following section is based.

2.1 Principles

Let's take two atoms. If one of the atom's nucleus emits a photon and goes from an excited to a ground state, one might assume that the other nucleus can absorb this photon because the excitation energy of both the nuclei is the same. But that is not the case, since energy is lost by the radiated photon because of the recoil of the nucleus, just like a gun recoils when a bullet is fired. In 1957, R. Mößbauer found that this energy reduction in the emitted photon can be reduced if the atom is part of the bigger crystalline structure. In such a situation, the recoil momentum is transferred to the crystal as a whole, which is much more massive than the atom itself and hence the recoil energy is negligible. The recoilless emission and absorption of γ -radiation by the nucleus of an atom is known as the Mößbauer effect [1]. This effect can be seen in Fig. 2.1.1.

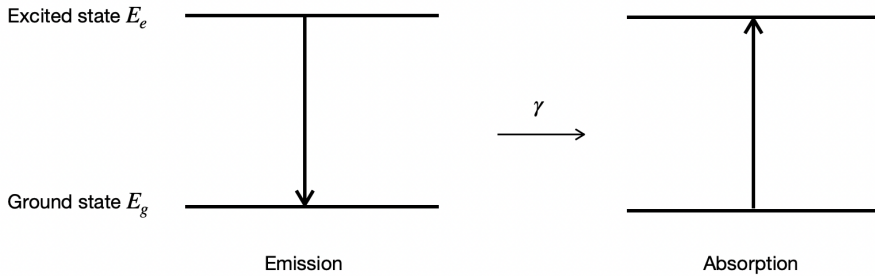


Figure 2.1.1: The recoilless emission and absorption of photon (Mößbauer effect).

2.1.1 Natural Linewidth

The uncertainty in energy in the case of recoilless emission is limited by its natural linewidth. From the Heisenberg's uncertainty principle, we know that

$$\Delta E \Delta t = \hbar, \quad (2.1.1)$$

where ΔE is the energy difference, Δt is the time difference and \hbar is the reduced Planck's constant. In our case, if we have a nuclear level with a mean lifetime of τ_N , the energy uncertainty is given by

$$\Gamma = \hbar / \tau_N. \quad (2.1.2)$$

The frequency spectrum given by this emitted γ -ray is given by a Lorentz distribution,

$$I(\omega) = \frac{I_0}{1 + [2\hbar(\omega - \omega_0)/\Gamma]^2} \quad (2.1.3)$$

where $I(\omega)$ is the intensity of the radiation at frequency ω . The distribution (Fig. 2.1.2) is centered at ω_0 and has a halfwidth of Γ/\hbar . For ^{57}Fe used in this experiment, $\Gamma = 4.7 \times 10^{-9}$ eV.

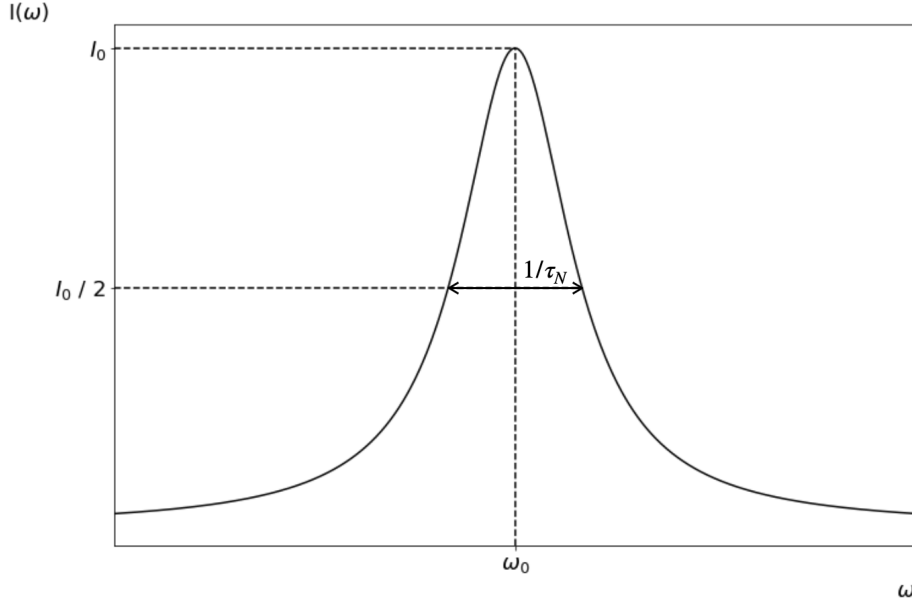


Figure 2.1.2: Intensity distribution of emitted γ -ray, centered at ω_0 with a halfwidth of $1/\tau_N$.

2.1.2 Recoil and Doppler Shift

As discussed in Section 2.1, the recoil of the nucleus when emitting a γ -ray leads to a reduced energy. This can be written as

$$E_{\text{before}} = E_e + \frac{p^2}{2M}, \quad (2.1.4)$$

where, p is the momentum and M is the mass of the nucleus. Energy after the emission can be written as

$$E_{\text{after}} = E_g + \frac{(p - \hbar k)^2}{2M}, \quad (2.1.5)$$

where $\hbar k$ is the momentum of the emitted γ -ray. The energy difference is

$$E_{\text{before}} - E_{\text{after}} \equiv \hbar\omega = \hbar\omega_0 + \hbar(k \cdot v) - \frac{\hbar^2 k^2}{2M}, \quad (2.1.6)$$

where the term $\hbar(k \cdot v)$ is the Doppler effect, which is responsible for shift and broadening of the spectra. At room temperature, the Doppler shift for ^{57}Fe is $\propto 10^{-2}$. The recoil energy $\hbar^2 k^2/2M$ is 2×10^{-3} eV, both of which are orders of magnitude greater than the natural width. The absorption and emission frequency spectrum is shown in Fig. 2.1.3.

2.1.3 Debye-Waller Factor

In a typical tightly bound solid, the energy required to displace an atom from its position is 20 eV. Since the recoil energy of the γ -ray is of the order 10^{-3} eV, there are two possibilities that can occur. One, since the atom cannot be displaced, it is set in a vibrational motion. Or second, if the vibrational motion is not altered by the emission, the recoil energy is absorbed by the entire solid. In a typical solid, the mass of the entire crystal is 10^{20} times more than the mass of the atom and hence the recoil energy is negligible. In this case, we get an unshifted, unbroadened, emission (Mößbauer) line.

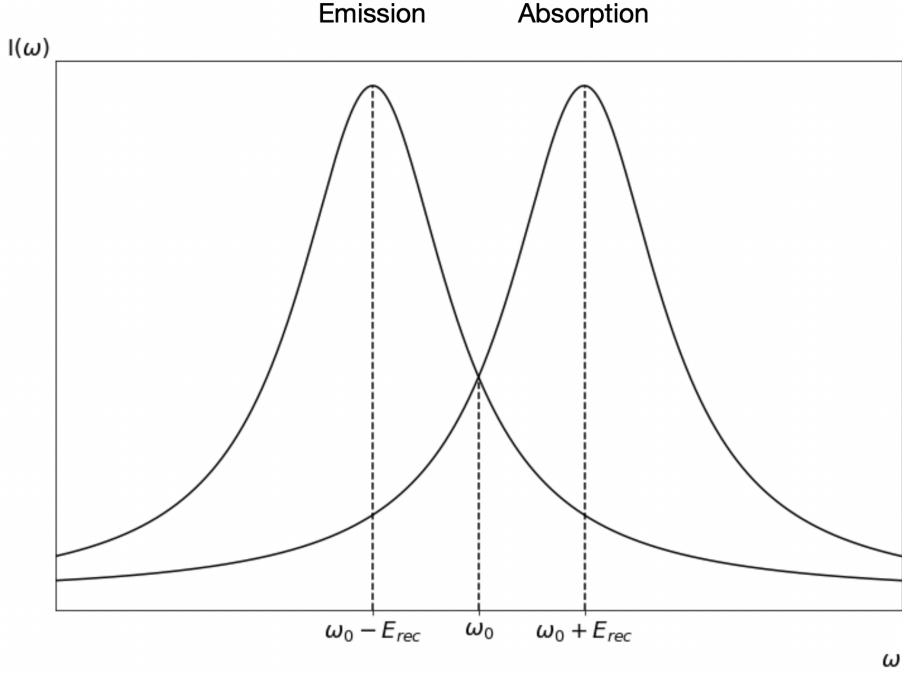


Figure 2.1.3: Emission and absorption spectrum of a monoatomic gas in thermal equilibrium. Both the spectra are shifted by the recoil energy and have been broadened due to Maxwell velocity distribution.

The Debye-Waller factor ($f(T)$) is defined as the ratio of the unshifted γ -ray emission to the total number of emissions. This ratio is dependent on temperature and is the highest at $T = 0\text{K}$. But even at absolute zero, $f < 1$. This is because of zero-point energy.

In order to understand the Mößbauer effect better, one needs to understand the Debye-Waller factor. Because this factor shows us why the Mößbauer fraction is large. Since the quantum mechanical derivation is a bit too complicated, we look at the semi-classical approach to gain an intuition behind the Debye-Waller factor.

The Semiclassical Approach of the Debye-Waller Factor

Let us consider a nucleus, continuously emitting an electromagnetic wave of frequency $\omega_0 = E_\gamma/\hbar$ and oscillating around an equilibrium point. Considering only one vibration frequency Ω , which corresponds to the Einstein model of the oscillations. The electric field of the emitted radiation is given by

$$E(t) = E_0 \exp(-i[\omega_0 t + kx(t)]), \quad (2.1.7)$$

where $x(t) = a \sin(\Omega t)$, a is the amplitude of the oscillation. Decomposition of this relation in Eqn. 2.1.7 shows that, the effect of vibration of the atom reduces the intensity of the central line by a factor of $(1 - k^2 a^2/4)$ and also produces sidebands with frequencies $\omega_0 \pm \Omega$, $\omega_0 \pm 2\Omega$, ...

If we sum up these contributions to the intensity from sidebands to the unshifted line, we get

$$A(\omega_0) = 1 - \frac{k^2 a^2}{4} + \dots = \mathcal{J}_0(ka), \quad (2.1.8)$$

where $\mathcal{J}_0(ka)$ is the Bessel function of zero order. The Debye-Waller factor is given by the absolute square of this quantity.

So far we have considered only a single oscillation mode. When we consider several normal modes (phonons), in which each frequency produces its own sidebands, we need to take the product of all of them (Eqn. 2.1.9).

$$f = \prod \mathcal{J}_0^2(ka_n) \approx \prod \left(1 - \frac{k^2 a_n^2}{4}\right)^2 \approx \exp(-k^2 \langle x^2 \rangle), \quad (2.1.9)$$

where $\langle x^2 \rangle = \sum a_n^2/2$ is the average square displacement. For an isotropic, 3-dimensional oscillator,

$$f = \exp\left(-\frac{k^2 \langle u^2 \rangle}{3}\right), \quad (2.1.10)$$

where $\langle u^2 \rangle = 3 \langle x^2 \rangle$, the average square displacement. In quantum mechanics, this $\langle u^2 \rangle$ becomes the expectation value.

Going back to the Einstein model, where only single vibration frequency Ω is considered, we can derive the temperature dependence for the Debye-Waller factor. The harmonic energy with n excited quanta is taken, the occupation probability is calculated and we find that the Bose-Einstein distribution function is obtained. Using this result, we then generalize for a phonon distribution function $Z(\Omega)$ and calculate the dependence for 3-dimensions. The result we obtain is

$$f(T) = \exp\left(-\frac{\hbar k^2}{6MN} \int_0^\infty \frac{Z(\Omega)}{\Omega} \left[1 + \frac{2}{\exp(\hbar\Omega/k_b T) - 1}\right] d\Omega\right), \quad (2.1.11)$$

where N is the number of molecules in the solid.

The following important conclusions can be deduced:

1. By measuring the Debye-Waller factor, one can obtain the phonon frequency spectrum.
2. The Debye-Waller factor decreases with increase in the recoil energy.
3. Large Mößbauer effect can be observed at low temperatures, which is because of the fact that the Debye-Waller factor is maximum at absolute zero. Hence, low temperatures are favorable for measurement.

2.2 Mößbauer Source

There are several requirements for a Mößbauer source. These are:

1. The γ -ray transition must go to the ground state, since for a stable isotope, absorption can only take place from the ground state.
2. The Debye-Waller factor must not be too small. In order to achieve that, we must have low temperatures, low γ -ray energy, high Debye temperature and high atomic mass.
3. The lifetime should not be too short, otherwise due to Eqn. 2.1.2, we will have a poor energy resolution.
4. The source should be practical (easy to obtain, handle and so on).

There are several possible sources for studying the Mößbauer effect, many of these are discussed in detail in [1]. In this experiment, we used isotope ^{57}Co as the source. The decay scheme is shown in Fig. 2.2.1.

The Mößbauer source $^{57}\text{Co}-^{57}\text{Fe}$ is an ideal choice because the parent isotope, ^{57}Co has long halflife (270 days), which enables one to perform several experiments with the same source. The lifetime of the Mößbauer level is sufficiently long, giving us a good energy resolution. Lastly, the energy level of 14.4 keV is small enough to allow for the conduction of experiment at room temperature.

2.3 Mößbauer Apparatus and Setup

A schematic representation of the setup is shown in Fig. 2.3.1. Here, we have a radioactive source, an absorber and a detector. In the diagram, the source is moving with respect to the absorber but in our setup, the source was stationary and the absorber was moving. This doesn't really change anything, since the relative motion is constant.

There are two possible arrangements: transmission geometry and scattering geometry. In transmission geometry, we record the intensity of γ -rays transmitted. While in scattering geometry, the fluorescence radiation is measured. In order to achieve the resonance condition (similar to what can be seen in Fig. 2.3.1), we move the absorber relative to the source (or vice versa). A loudspeaker principle

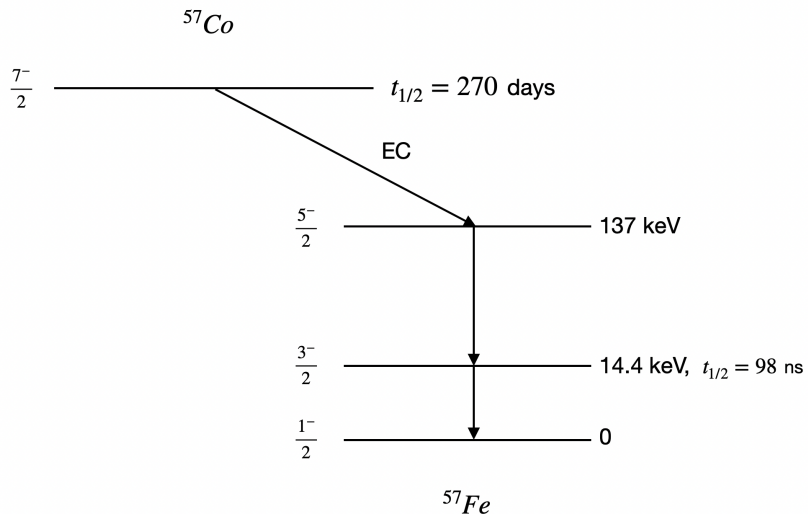


Figure 2.2.1: Decay scheme of ^{57}Co . The decay occurs largely (99.8%) due to Electron Capture (EC). The nuclear moments of Mößbauer level ($I = 3/2$) and ground level ($I = 1/2$) are shown here.

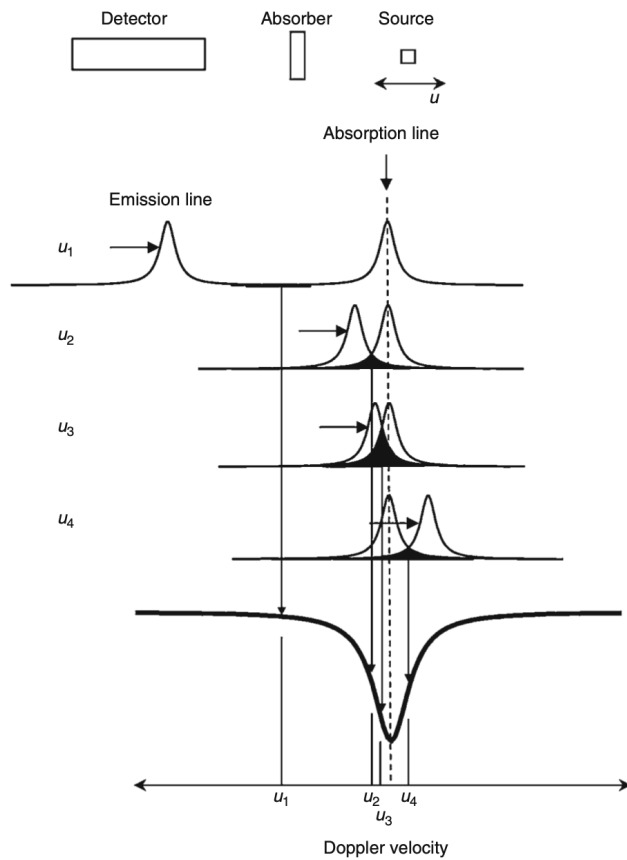


Figure 2.3.1: A representation of the setup of the experiment. In our case, the absorber moves while the source remains stationary. The Doppler principle is seen by the scanning of the absorption line with the emission line. The resultant intensity is proportional to the addition of absorption and emission lines, which are marked at four arbitrary chosen velocities between u_1 and u_4 [2].

is often used to produce these oscillations. On these oscillations, velocity profiles can be imposed by using driver coils, using a function generator.

The γ -ray detector is often made of scintillators or gas-filled proportional counters. These detect the intensity of γ -rays that pass through the absorber. The pulse height that we get with a proportional counter with 97% Kr and 3% CO₂, is shown in Fig. 2.3.2. The line corresponding to 14.4 keV is the Mößbauer line. This is the region that we study in the experiment in order to get the Mößbauer spectrum.

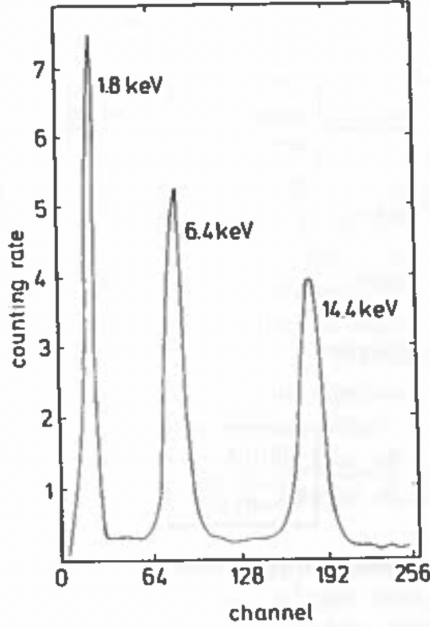


Figure 2.3.2: Pulse height spectrum measured using gas-filled proportional counter. The 14.4 keV Mößbauer line is shown. [1].

The absorber velocity is varied from 0 mm/s to 6 mm/s. The counts for the γ -rays are recorded separately for when it is moving Left-to-Right (LR), N(LR) and when it is moving Right-to-Left (RL), N(RL). Depending upon the direction of motion of the absorber, the detector pulses are fed into the signal-channel-analyzer into their respective counters. At the same time, the respective timers feed their information into the counters of their respective channel, T(LR) or T(RL). The number of turns made by the absorber can be read off from the run counter. The total swing of the device is 25.1mm.

2.4 Isomer Shift

A shift in the resonance of the spectrum occurs in the Mößbauer experiment due to difference in the monopole energy in the ground state and excited state. The monopole energy is given by

$$E_c = \frac{Ze^2}{6\epsilon_0} |\Psi(0)|^2 \langle r^2 \rangle, \quad (2.4.1)$$

where $\langle r^2 \rangle$ is the mean square radius of the nuclei.

For a moving absorber, the energy difference between excited (e) to ground state (g) is given by

$$\hbar\omega(A) = \hbar\omega_0 \left(1 + \frac{v}{c}\right) + \frac{Ze^2}{6\epsilon_0} |\Psi_A(0)|^2 (\langle r_e^2 \rangle - \langle r_g^2 \rangle), \quad (2.4.2)$$

where the first term corresponds to Doppler shift due to the motion of the absorber. For a stationary absorber,

$$\hbar\omega(S) = \hbar\omega_0 + \frac{Ze^2}{6\epsilon_0} |\Psi_S(0)|^2 (\langle r_e^2 \rangle - \langle r_g^2 \rangle). \quad (2.4.3)$$

For the resonance condition to be fulfilled, $\omega(S) = \omega(A)$, the velocity of the absorber must be

$$v_{res} = \frac{Ze^2c}{6\epsilon_0\hbar\omega_0} \left(|\Psi_A(0)|^2 - |\Psi_S(0)|^2 \right) \left(\langle r_e^2 \rangle - \langle r_g^2 \rangle \right), \quad (2.4.4)$$

where v_{res} is the isomer shift. By convention, this value is positive when the absorber is moving near the source. For ^{57}Fe , this value is negative since the radius of the nuclei in the excited state is smaller than the of ground state. Typically, the order of isomer shift is of the order of several mm s^{-1} .

2.5 Electric Quadrupole Interaction

Electric quadrupole interaction occurs in the presence of electric field gradient, which leads to non-spherical nucleus when the nuclear spin $I \geq 1$. In this case the degeneracy of the m sublevels is lifted and we get a splitting of energy levels. As can be seen in Fig. 2.5.1, the energy level splitting does not depend on the sign of m , $m = \pm 3/2$ are indistinguishable.

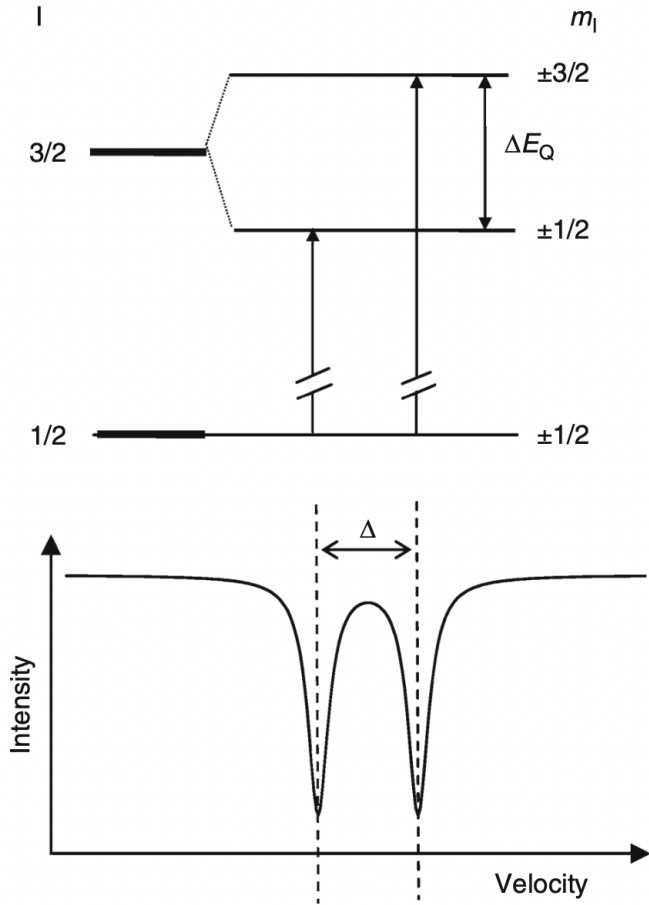


Figure 2.5.1: Quadrupole splitting of $I = 3/2$ and the corresponding Mößbauer spectrum [2].

The energy separation that can be seen Fig. 2.5.1, is given by

$$\Delta E = 6\hbar\omega_Q = \hbar\omega_0 \frac{\Delta v}{c}, \quad (2.5.1)$$

where Δv is the separation in between two lines in velocity spectrum, it is given by

$$\Delta v = \frac{eQV_{zz}c}{2\hbar\omega_0}. \quad (2.5.2)$$

In the case of powder sample of ^{57}Fe , we get equal amplitude of Mößbauer lines. This is because the electric field gradient are distributed statistically, which leads to the γ -rays being emitted isotropically.

2.6 Magnetic Dipole Interaction

Magnetic dipole interaction leads to further splitting in the energy levels of the sublevels. This is a result of magnetic interaction ($-\mu \cdot B$) splitting the magnetic sublevels equally, consequently splitting the energy levels of the emitted γ radiation. Fig. 2.6.1 shows the magnetic splitting for ^{57}Fe .

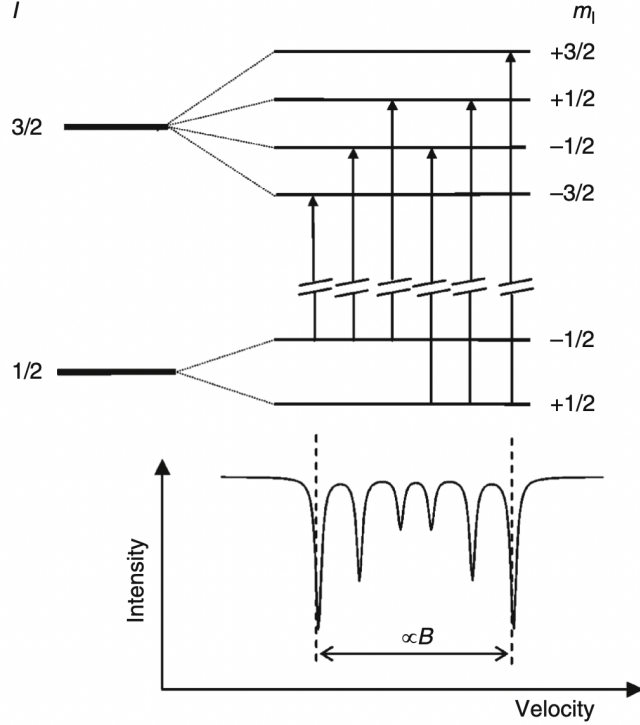


Figure 2.6.1: The magnetic splitting of energy levels and the corresponding Mößbauer spectrum of ^{57}Fe [2].

Experimentally, only six lines are transitions are observed and therefore we can conclude that this follows the m_1 selection rules, according to which no m cannot be greater than one. The transition energies are given by

$$\hbar\omega(m_e \rightarrow m_g) = \left(E_e - \frac{\mu_e}{I_e} m_e B \right) - \left(E_g - \frac{\mu_g}{I_g} m_g B \right) \quad (2.6.1)$$

$$= \hbar\omega_0 - \left(\frac{\mu_e}{I_e} m_e - \frac{\mu_g}{I_g} m_g \right) B. \quad (2.6.2)$$

The resonant velocity is given by

$$v_{res} = -\frac{c}{\hbar\omega_0} \left(\frac{\mu_e}{I_e} m_e - \frac{\mu_g}{I_g} m_g \right) B. \quad (2.6.3)$$

The magnetic hyperfine structure can be given by

$$H = -\mu \cdot B = -g\mu_N I B, \quad (2.6.4)$$

where μ is the magnetic moment and μ_N is the nuclear nuclear magneton [2]. Since the magnetic energy is given by $E_m = g\mu_N M B$, the energy perturbation due to hyperfine splitting is given by

$$E_m = -g\mu_N B. \quad (2.6.5)$$

Chapter 3

Experimental Set-Up

To measure the Moessbauer spectrum, we placed a Co-57 radioactive source onto a table with a moving absorber that has a maximum displacement of 25.1 ± 0.2 mm. A photodetector is placed behind the absorber that detects the number of photons that are not absorbed via this process. The speed of the absorber is controlled by a motor that swings the absorber at a fixed velocity. See Fig. 3.0.1 for the Moessbauer source apparatus.

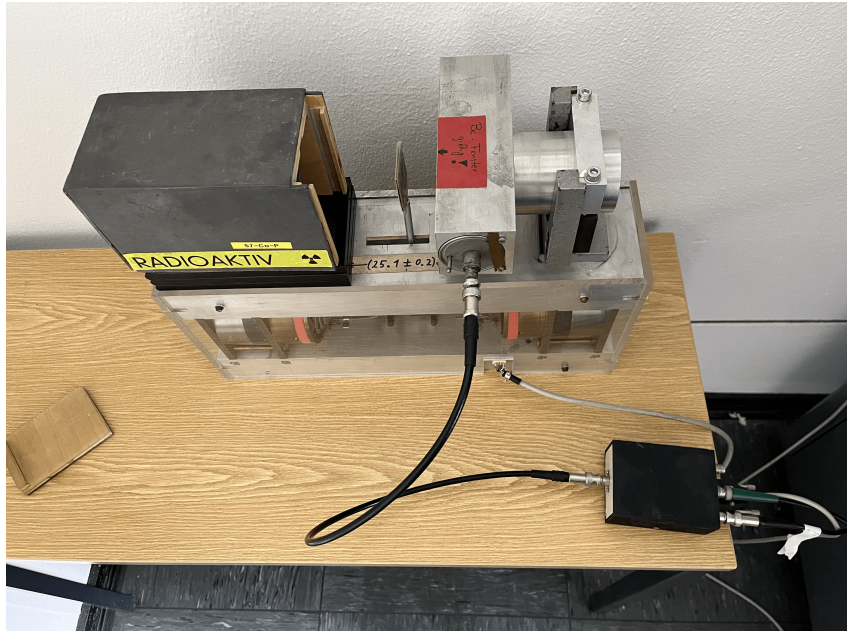
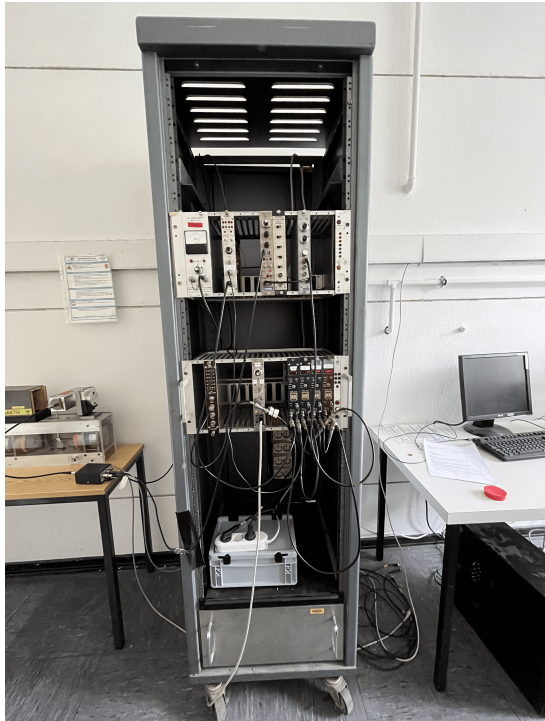
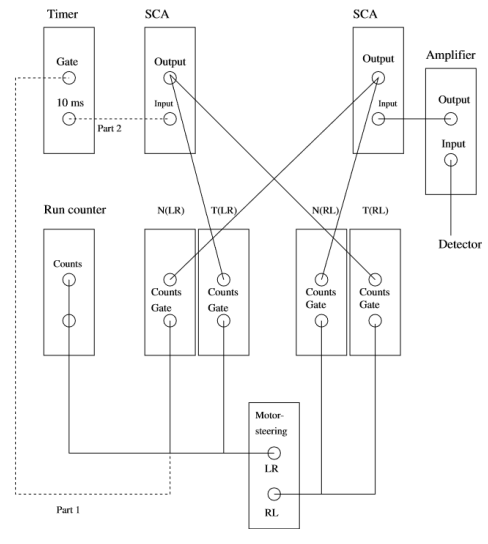


Figure 3.0.1: The set-up of the Moessbauer source. *Left:* The Co-57 source. *Middle:* The moving absorber. *Right:* The photodetector which is connected to the detector apparatus.

The photodetector is then connected to a single channel analyzer (SCA), which determines the number of counts detected in a given time range and maximal and minimal width to observe the counts. The SCA has 2 main parameters that should be modified: the Upper Level Discriminator (ULD) and the Lower Level Discriminator (LLD), which controls the binsize and the lower limit for photodetection respectively. The modes of the ULD can be set to measure with a higher resolution by detecting counts with 10 % of the binsize. The SCA was then connected to a display in which the number of counts obtained in a specific time interval was shown. The photodetecting apparatus consisted of two such setups to consider for measurements with positive and negative velocity of the absorber as the offset voltage between the two can allow the measurements in the LR and RL direction to differ. A separate run counter that tracks the number of turns that the absorber had is also contained in the apparatus. A timer that controls the time interval of measurement is also placed which is used for the calibration process. The set-up is constructed in a way such that the count and time measurements terminate only after the absorber had performed a full turn. See Fig. 3.0.2 for the apparatus used for the photodetection as well as the schematic of the apparatus.



(a)



(b)

Figure 3.0.2: (a) The photodetector apparatus used in this experiment. (b) The schematic of the apparatus. Obtained from Ref. [3].

Chapter 4

Calibration

Before we took any measurements, we determined the optimal values for the LLD in order to ensure that we are detecting counts from the 14.4 keV transition. In order to do so, we modified the LLD from 0 to 4 and determined the number of counts obtained at each value for a fixed time interval for $T = 10$ s. Once the data was obtained, we plotted the number of detected photons N against the LLD values and compared our results to the Fe-57 γ -spectrum as seen in Fig. [add reference here](#). This allowed us to identify the range in which we should set the ULD and LLD values when performing the Moessbauer measurements. Fig. 4.0.1 shows the obtained spectrum from our experiment. See the Appendix section for the full data obtained from this section. The uncertainty for the counts were taken to be purely statistical such that $\delta N = \sqrt{N}$, and the uncertainty of the time interval measurement was taken to be $\delta T = \pm 0.003$ s.

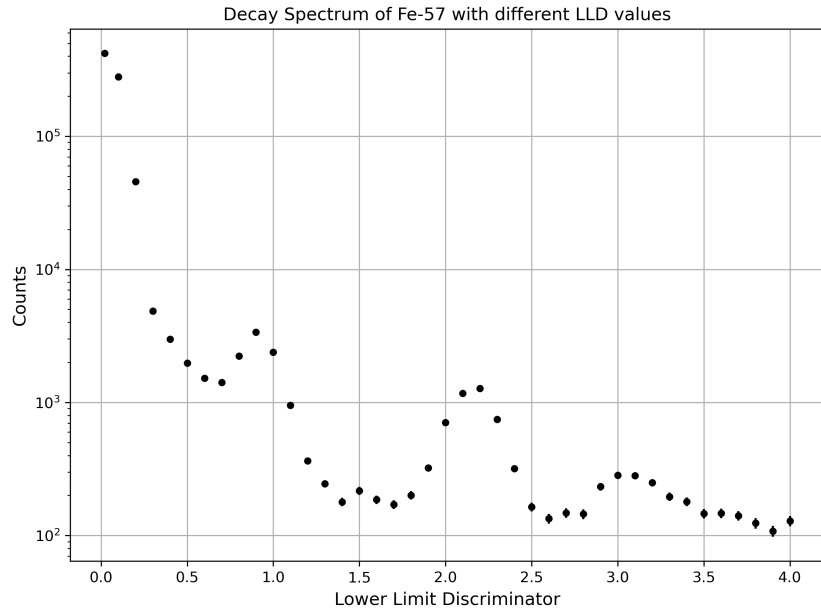


Figure 4.0.1: The pulse height spectrum for Fe-57 decay observed in the experiment. The number of counts are shown for varying LLD values.

By comparison to expected results, we identified the 14.4 keV transition line as the third peak on Fig. 4.0.1. The ULD and LLD values that were used to perform the Moessbauer measurement was then set to be 1.8 and 2.6 respectively.

Chapter 5

Moessbauer Spectrum

5.1 Spectrum

To observe the Moessbauer spectrum, we first set the ULD and LLD to 1.8 and 2.6 respectively as obtained from Chapter 4. Once a certain motor speed has been set, we ran both LR and RL single channel analyzer for a set number of turns, ranging from 4 to 10 turns. We then recorded the obtained number of counts and duration for both LR and RL analyzers. This was repeated until we obtained enough points to more accurately construct the Moessbauer peaks. This was verified by using the built-in plotting tool in Excel where we displayed the plot between the count rate $R = N/T$ against the motor speed. We took a total of 60 measurements in this experiment, ranging for motor speeds from 0 to 2.5. Fig. 5.1.1 shows the raw data obtained from both analyzers. See Appendix (Chapter 8) for the raw data table obtained from both analyzers.

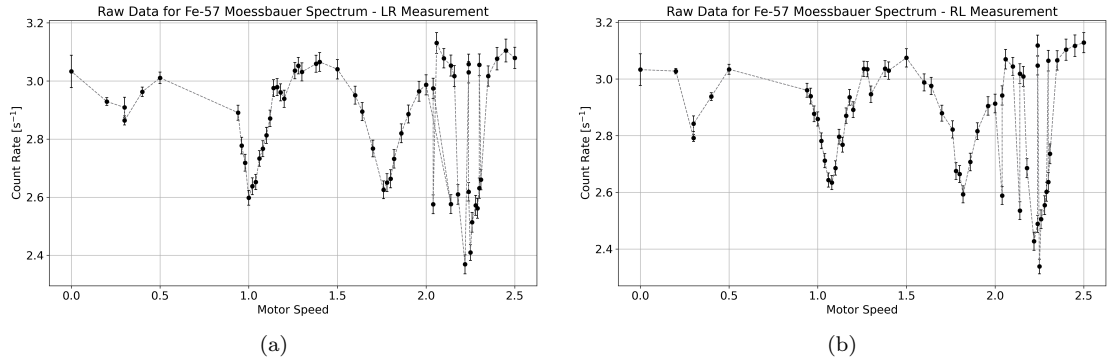


Figure 5.1.1: The Raw Spectrum obtained from the Moessbauer measurement for the 14.4 keV transition for Fe-57 from the (a) LR and (b) RL single channel analyzer. Several outliers can be observed.

The uncertainty of the count rate was calculated using the standard Gaussian error propagation formula using δN , δT as in Chapter 4:

$$\delta R = R \sqrt{\left(\frac{\delta N}{N}\right)^2 + \left(\frac{\delta T}{T}\right)^2} = R \sqrt{\left(\frac{\sqrt{N}}{N}\right)^2 + \left(\frac{\delta T}{T}\right)^2}. \quad (5.1.1)$$

To determine the peaks, we first filtered out the outliers from the data, then combined the LR and RL measurements to construct the full Moessbauer spectrum. We then performed a non-linear fit to the multi-Lorentzian distribution, i.e. the sum of Lorentzian distributions, to determine the peak velocity v_0 , peak amplitude I_0 , and uncertainty Γ_v for each observed peak. The offset δ_I from a full symmetric distribution was also determined through this fitting process. The equation used to fit is shown as such:

$$I_{tot}(v, v_{0_i}, I_{0_i}, \Gamma_{v_i}, \delta_I) = \delta_I + \sum_{i=1}^{N_{\text{peaks}}} -I_{0_i} \frac{(\Gamma_{v_i}/2)^2}{(v - v_{0_i})^2 + (\Gamma_{v_i}/2)^2} \quad (5.1.2)$$

The fitting procedure was implemented using the Python package `lmfit` which utilizes the Levenberg-Marquardt method. Fig. 5.1.2 shows the full Moessbauer spectrum with the obtained Lorentzian fit, and Table 5.1 shows the obtained fit parameters from the analysis for each peak. The offset was determined to be $\delta_I = 3.162 \pm 0.025 \text{ s}^{-1}$. The uncertainties were obtained from the covariance matrix evaluated through the fitting procedure.

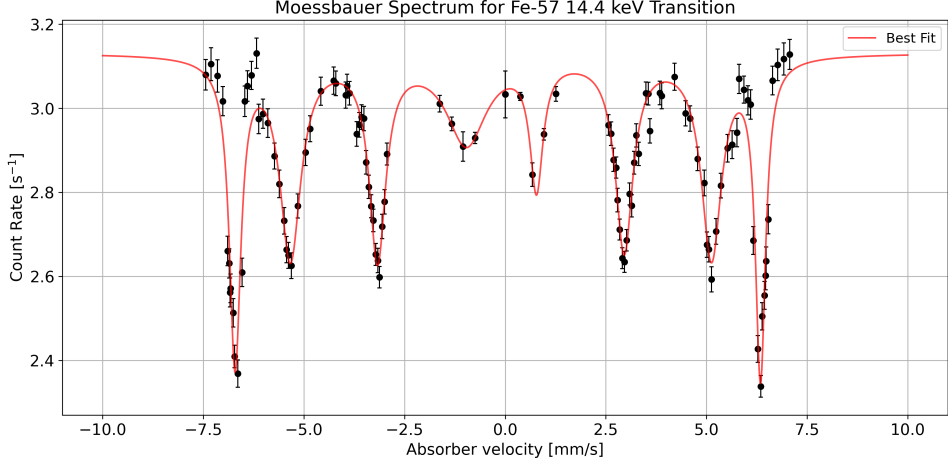


Figure 5.1.2: The observed Moessbauer spectrum for Fe-57 through the 14.4 keV transition for varying absorber velocities. The non-linear Lorentzian fit is also shown.

Peak	v_0 [mm s ⁻¹]	I_0 [s ⁻¹]	Γ_v [mm s ⁻¹]	$\delta_v - I_0$ [s ⁻¹]
1	-6.7131 ± 0.0097	0.759 ± 0.039	0.352 ± 0.033	2.403 ± 0.046
2	-5.335 ± 0.026	0.501 ± 0.036	0.682 ± 0.096	2.661 ± 0.043
3	-3.174 ± 0.016	0.487 ± 0.030	0.538 ± 0.066	2.674 ± 0.039
4	-0.94 ± 0.14	0.226 ± 0.034	1.54 ± 0.77	2.935 ± 0.042
5	0.776 ± 0.033	0.311 ± 0.080	0.43 ± 0.20	2.851 ± 0.084
6	2.958 ± 0.015	0.476 ± 0.028	0.583 ± 0.064	2.685 ± 0.038
7	5.124 ± 0.025	0.496 ± 0.034	0.673 ± 0.094	2.666 ± 0.042
8	6.3449 ± 0.0089	0.770 ± 0.038	0.315 ± 0.029	2.392 ± 0.045

Table 5.1: Fit parameters v_0 , I_0 , and Γ_v obtained for each peak. The peak values $\delta_v - I_0$ as shown in Fig. 5.1.2 is also presented. The peak is numbered from the left most peak to the rightmost peak.

From Fig. 5.1.2, we observe a total of eight peaks, contrary to the six peaks that are expected from the hyperfine splitting of the Fe-57 spectrum. After calculating for the isomer shift and g-factors in the following sections, we observed that the first and last peaks were outliers that may have not have been a result of the 14.4 keV transition of Fe-57. A possible explanation of the additional peaks is due to the oxidation of the absorber. As the instrument may be relatively old, the iron may have oxidized, creating impurities within the absorber. The oxidation of the iron will have caused some of the iron to iron(III) oxide, containing Fe_2O_3 , FeO , and Fe_3O_4 . When performing Moessbauer spectroscopy onto such molecules, one observes finer splitting at absorber velocities of around $6 - 8 \text{ mm s}^{-1}$, which is what we also observe from Fig. 5.1.2 [4]. In the following sections, we will omit the parameters obtained from the first and last peaks.

5.2 Natural Linewidth

To compare the obtained peaks to the analytical results from the hyperfine splitting of the Fe-57 nucleus through the 14.4 keV transition, we convert the fit parameters described in the absorber velocity into the transition energy E_γ using the equation describing the Doppler shift of the ground state energy:

$$E = E_0 \left(1 + \frac{v}{c}\right) \implies \Delta E = E_\gamma = E_0 \frac{v}{c} \quad (5.2.1)$$

where E_0 is the expected ground state energy $E_0 = 14.4 \text{ keV}$. The linewidths were converted in a similar fashion. Table 5.2 shows the energy value ΔE and its linewidth Γ for each observed peak.

Peak	$\Delta E [1 \times 10^{-7} \text{ eV}]$	$\Gamma [1 \times 10^{-9} \text{ eV}]$
1	-3.2223 ± 0.0046	8.4 ± 0.8
2	-2.561 ± 0.012	16.3 ± 2.3
3	-1.5238 ± 0.0079	12.9 ± 1.5
4	-0.453 ± 0.069	36 ± 18
5	0.372 ± 0.015	10.2 ± 4.9
6	1.4201 ± 0.0073	14.0 ± 1.5
7	2.460 ± 0.012	16.1 ± 2.2
8	3.0456 ± 0.0043	7.5 ± 0.6

Table 5.2: The energy values at the peaks ΔE and the linewidths Γ obtained for each peak. The peaks are labelled as given in Table 5.1.

From Table 5.2, we obtained an average linewidth of $\Gamma_{\text{avg}} = 35.5 \pm 6.5 \text{ eV}$. Comparing this to the natural linewidth of the 14.4 keV transition of $\Gamma_0 =$, we observe that the linewidths we obtained are an order of magnitude larger. A possible cause for this may be due to the Doppler broadening that is caused by temperature fluctuations

Chapter 6

Conclusion and Outlook

Chapter 7

Acknowledgements

We would like to take this moment and thank Dr. Barth, who was really helpful and patient with us. We were lucky to have him as our tutor. Next, we would like to thank...

Bibliography

- [1] G. Schatz, G. Schatz, A. Weidinger, and J. Gardner, *Nuclear Condensed Matter Physics: Nuclear Methods and Applications*. Wiley, 1996, ISBN: 9780471954798. [Online]. Available: <https://books.google.de/books?id=xMDvAAAAMAAJ>.
- [2] E. Kuzmann, Z. Homonnay, S. Nagy, and K. Nomura, “Mössbauer spectroscopy,” in *Handbook of Nuclear Chemistry*, A. Vértes, S. Nagy, Z. Klencsár, R. G. Lovas, and F. Rösch, Eds. Boston, MA: Springer US, 2011, pp. 1379–1446, ISBN: 978-1-4419-0720-2. DOI: [10.1007/978-1-4419-0720-2_25](https://doi.org/10.1007/978-1-4419-0720-2_25). [Online]. Available: https://doi.org/10.1007/978-1-4419-0720-2_25.
- [3] P. A. L. Course, *K221 mößbauer effect*, Jul. 2016.
- [4] J. Winsett, A. Moilanen, K. Paudel, *et al.*, “Quantitative determination of magnetite and maghemite in iron oxide nanoparticles using mössbauer spectroscopy,” *SN Applied Sciences*, vol. 1, no. 12, p. 1636, Nov. 2019, ISSN: 2523-3971. DOI: [10.1007/s42452-019-1699-2](https://doi.org/10.1007/s42452-019-1699-2). [Online]. Available: <https://doi.org/10.1007/s42452-019-1699-2>.

Chapter 8

Appendix

In the following section, we include all the data which was measured while performing the experiment.
Verify the unit of motor speed.

LLD \pm 0.01	Count (N)	Time (s) \pm 0.03	ULD (ΔE) (100%) (10^{-1})
0.02	420580	10	10
0.10	279704	10	10
0.20	45643	10	10
0.30	4853	10	10
0.4	2982	10	10
0.5	1981	10	10
0.6	1522	10	10
0.7	1412	10	10
0.8	2227	10	10
0.9	3368	10	10
1	2386	10	10
1.1	952	10	10
1.2	365	10	10
1.3	245	10	10
1.4	179	10	10
1.5	217	10	10
1.6	186	10	10
1.7	171	10	10
1.8	201	10	10
1.9	322	10	10
2	705	10	10
2.1	1169	10	10
2.2	1275	10	10
2.3	745	10	10
2.4	319	10	10
2.5	164	10	10
2.6	134	10	10
2.7	148	10	10
2.8	145	10	10
2.9	233	10	10
3	284	10	10
3.1	282	10	10
3.2	249	10	10
3.3	196	10	10
3.4	180	10	10
3.5	146	10	10
3.6	147	10	10
3.7	141	10	10
3.8	124	10	10
3.9	108	10	10
4	129	10	10

Table 8.1: Calibration of the single channel analyzer. Where, Lower Limit Discriminator (LLD) and Upper Level Discriminator (ULD).

Velocity (mm/s)	Motor speed (V)	Count (N)	Time (ms)	Turns	Count/s (N/s)
0	0	3030	999	0	3.03303303303303
0.375400077772128	0.2	101223	33431	5	3.02781849181897
0.674368619022031	0.3	10578	3722	1	2.8420204191295
0.959174574867843	0.4	46130	15701	6	2.9380294248774
1.25827150591538	0.5	30264	9974	5	3.03428915179467
2.56488861639076	0.94	14484	4893	5	2.96014714898835
2.62964903090623	0.96	11223	3818	4	2.93949711891042
2.68952585052237	0.98	10741	3733	4	2.87731047414948
2.7564243356029	1	13016	4553	5	2.85877443443883
2.79276773296245	1.02	10000	3595	4	2.78164116828929
2.84580498866213	1.04	11958	4410	5	2.71156462585034
2.90913305516922	1.06	11403	4314	5	2.6432545201669
2.96340023612751	1.08	11156	4235	5	2.63423848878394
3.01827801827802	1.1	11168	4158	5	2.68590668590669
3.09037182959862	1.12	11355	4061	5	2.79610933267668
3.14142678347935	1.14	11058	3995	5	2.76795994993742
3.19989801121877	1.16	11258	3922	5	2.87047424783274
3.25551232166018	1.18	11316	3855	5	2.93540856031128
3.31659619450317	1.2	10942	3784	5	2.89164904862579
3.49663338750871	1.26	13076	4307	6	3.03598792663107
3.55608028335301	1.28	12852	4235	6	3.03471074380165
3.59701920321009	1.3	10279	3489	5	2.94611636572084
3.84085692425402	1.38	11906	3921	6	3.03647028819179
3.89026658400496	1.4	9773	3226	5	3.02944823310601
4.20576407506702	1.5	9175	2984	5	3.07473190348525
4.47814451382694	1.6	10048	3363	6	2.98780850431163
4.59146341463415	1.64	9760	3280	6	2.97560975609756
4.78225367446924	1.7	10579	3674	7	2.87942297223734
4.94418910045962	1.76	8596	3046	6	2.8220617202889
5.0133155792277	1.78	8037	3004	6	2.6754327563249
5.06218487394958	1.8	7927	2975	6	2.66453781512605
5.12593601089176	1.82	7618	2938	6	2.5929203539823
5.24008350730689	1.86	7780	2874	6	2.70702853166319
5.35997559487492	1.9	9231	3278	7	2.81604636973764
5.52660550458716	1.96	7916	2725	6	2.90495412844037
5.64044943820225	2	7779	2670	6	2.91348314606742
5.7546809323653	2.04	7699	2617	6	2.94191822697746
5.81018518518519	2.06	7957	2592	6	3.06983024691358
5.93180283592167	2.1	9017	2962	7	3.04422687373396
6.03123748498198	2.14	7538	2497	6	3.01882258710453
6.09716599190283	2.16	7432	2470	6	3.00890688259109
6.1620294599018	2.18	6563	2444	6	2.68535188216039
6.275	2.22	5826	2400	6	2.4275
6.32241813602015	2.24	6916	2779	7	2.48866498740554
6.35264341957255	2.25	8315	3556	9	2.33830146231721
6.38135593220339	2.26	5912	2360	6	2.50508474576271
6.44415917843389	2.28	5970	2337	6	2.55455712451861
6.46629454701589	2.29	6060	2329	6	2.60197509660799
6.4802065404475	2.3	6127	2324	6	2.63640275387263
6.53362255965293	2.31	6306	2305	6	2.73579175704989
6.64272211720227	2.35	8109	2645	7	3.06578449905482
6.77158273381295	2.4	6902	2224	6	3.10341726618705
6.92413793103448	2.45	6780	2175	6	3.11724137931034
7.06757843925986	2.5	7777	2486	7	3.1283185840708

Table 8.2: Velocity measurements for Right to Left (RL).

Velocity (mm/s)	Motor speed (V)	Count (N)	Time (ms)	Turns	Count/s (N/s)
-7.44176196526895	2.5	7271	2361	7	3.07962727657772
-7.31067961165049	2.45	6396	2060	6	3.10485436893204
-7.14760322733745	2.4	6483	2107	6	3.07688656858092
-7.0167731629393	2.35	7554	2504	7	3.0167731629393
-6.8956043956044	2.31	5810	2184	6	2.66025641025641
-6.854802002731	2.3	5780	2197	6	2.63086026399636
-6.83923705722071	2.29	5641	2202	6	2.56176203451408
-6.82065217391304	2.28	5678	2208	6	2.57155797101449
-6.75942549371634	2.26	5600	2228	6	2.51346499102334
-6.72521583804704	2.25	8093	3359	9	2.40934802024412
-6.64314071460079	2.22	5370	2267	6	2.36876929863255
-6.53362255965293	2.18	6015	2305	6	2.60954446854664
-6.47185217017619	2.16	7020	2327	6	3.01675977653631
-6.40033999150021	2.14	7184	2353	6	3.0531236719082
-6.30426982418371	2.1	8579	2787	7	3.07822030857553
-6.1771944216571	2.06	7633	2438	6	3.13084495488105
-6.12444082960553	2.04	7315	2459	6	2.97478649857666
-6.01437699680511	2	7479	2504	6	2.98682108626198
-5.89663273296789	1.96	7572	2554	6	2.96476115896633
-5.73059360730594	1.9	8849	3066	7	2.88617090671885
-5.61311964219158	1.86	7566	2683	6	2.81997763697354
-5.49434512951478	1.82	7489	2741	6	2.73221452024808
-5.43486106098881	1.8	7381	2771	6	2.66365932876218
-5.38241601143674	1.78	7415	2798	6	2.65010721944246
-5.31216931216931	1.76	7443	2835	6	2.62539682539683
-5.15098211668133	1.7	9440	3411	7	2.76751685722662
-4.96210873146623	1.64	8786	3035	6	2.89489291598023
-4.8486799742434	1.6	9166	3106	6	2.95106245975531
-4.57862094126231	1.5	8334	2741	5	3.04049616928128
-4.25856803529013	1.4	9035	2947	5	3.06582965727859
-4.20670391061453	1.38	10952	3580	6	3.05921787709497
-3.9652448657188	1.3	9594	3165	5	3.03127962085308
-3.92801251956182	1.28	11704	3834	6	3.05268648930621
-3.86748844375963	1.26	11822	3894	6	3.03595274781715
-3.68683901292597	1.2	10004	3404	5	2.93889541715629
-3.6229792147806	1.18	10256	3464	5	2.96073903002309
-3.57041251778094	1.16	10471	3515	5	2.97894736842105
-3.51147174034695	1.14	10635	3574	5	2.97565752658086
-3.45825296224855	1.12	10420	3629	5	2.87131441168366
-3.38731443994602	1.1	10422	3705	5	2.81295546558704
-3.33244822092406	1.08	10420	3766	5	2.76686139139671
-3.27847439916405	1.06	10463	3828	5	2.73328108672936
-3.21794871794872	1.04	10344	3900	5	2.65230769230769
-3.16320100819156	1.02	8372	3174	4	2.63768115942029
-3.12266733018164	1	10441	4019	5	2.59790992784275
-3.05817849527871	0.98	8925	3283	4	2.71855010660981
-2.99880525686977	0.96	9299	3348	4	2.77747909199522
-2.93429974281038	0.94	12364	4277	5	2.89081131634323
-1.62902388369678	0.5	23197	7704	5	3.01103322949117
-1.33003620948512	0.4	33549	11323	6	2.96290735670759
-1.04496253122398	0.3	6987	2402	1	2.90882597835137
-0.746668253212756	0.2	49236	16808	5	2.92931937172775
0	0	3030	999	0	3.03303303303303

Table 8.3: Velocity measurements for Left to Right (LR).